The Sand Coated Die

F. MAMPAEY - Foundry Research Centre, Grote Steenweg Noord 2 - B 9710, Zwijnaarde Ghent, Belgium

Summary

The sand coated die is composed of a casting and a die which are separated by a layer of variable sand thickness. Increasing sand thickness will reduce the chilling influence of the die and hence augment the solidification time of the casting. A computer model has been developed which accurately predicts the relative solidification time in the sand coated die. This model, validated for several cast metals, is in close agreement with the experimental data of the present research as well as with the ones published previously in literature. At the interface sand – die no perfect conduction contact exists. This may be explained by a simplified model of sand grains packing.

Riassunto

Lo stampo rivestito di sabbia consiste in una fusione ed uno stampo separati fra di loro da uno strato di sabbia di spessore variabile. Incrementando detto spessore, si riduce l'effetto raffreddante esercitato dallo stampo, aumentando di conseguenza il tempo di solidificazione della fusione. È stato sviluppato un modello matematico che offre una precisa indicazione del tempo relativo di solidificazione in uno stampo rivestito di sabbia. Questo modello è stato validato su diverse leghe da fonderia. I risultati sono in stretto accordo con quelli sperimentali descritti sia nella lettura che nella presente relazione. Il contatto imperfetto di conducibilità osservato alla interfaccia sabbia-stampo viene giustificato con l'aiuto di un modello semplificato della compattazione dei granelli di sabbia.

1. Introduction

The sand coated die is composed of a casting and a die which are separted by a layer of variable sand thickness. Increasing sand thickness will reduce the chilling influence of the die and hence augment the solidification time of the casting. Industrial applications of this technique have been reported by Snezhnoi et al [1]. According to these authors, the sand coated die allows to reduce the amount of sand by a factor 10 to 20. Only a very limited number of publications are available in literature which deal with the influence of the sand thickness on the cooling rate of castings. Böhm [2] applied the method for massive steel castings with plate thickness between 50 and 300 mm. Schürmann et al [3] studied lamellar graphite castings with plate thickness of 9 and 19 mm, including the effect of the cooling rate on the form and the length of the graphite flakes and the type of the matrix [4]. These experiments demonstrate the feasibility of the method to alter the solidification sequence in a casting to some extent by applying different sand thicknesses at various casting locations. The results [2, 3] will be reviewed more detailed when comparing them with the ones obtained in the present investigation. The present study does not aim to weigh up pros and cons of the sand coated die casting technique since these were discussed previously [2]. Experimental results for different casting alloys will be used to validate a general simulation model. Simulation results of this model will be compared with the data published by Böhm and Schürmann.

2. Experimental procedure

The experimental arrangement of the sand coated die is shown schematically in fig. 1. Mould and die are vertically mounted on a gravity die casting machine with a variable locking force. Free convection of the air is allowed at the external die planes. Dies are made of lamellar graphite cast iron. The use of

several dies allows to vary the sand thickness between 5 and 40 mm. The casting thickness equals 20 or 30 mm. AFS 75 silica sand was bonded with silicate when pouring steel, with furan resin for aluminium and with pep-set for cast iron. Moulds were prepared by putting the pattern plate between the two die halves and filling it with the sand mixture from the top. During moulding the pattern plate is vibrated while maintaining a low locking force between the die halves. Reference castings were produced in full sand moulds with sand thickness of 75 or 150 mm. After hardening of the sand, the pattern plate is taken away and a thermocouple is located in the middle of the casting. The Pt — Pt Rh (10%) thermocouple is protected in a 3 mm quartz tube. Temperature has been recorded digitally. During pouring, the maximum locking force of 200 kN is maintained.

Aluminium-silicon alloy was melted from a master alloy in a graphite crucible which was placed in a medium frequency furnace. No modification treatment was adopted. After solidification next analysis was obtained (weight percent):

Si 13.2%; Cu 0.05%; Fe 0.36%; Mg 0.007%.

Spheroidal graphite cast iron was induction melted and treated with a Ni-Mg alloy at 1550°C. Inoculation was done with a Ce-Bi based ferro-silicon alloy (Spherix). Final composition ranges between: 3.45 - 3.68% C; 2.8 - 3.0% Si; 0.02% Mn; 0.03% P; 0.006 - 0.011% S; 0.6 - 0.8% Ni; 0.033 - 0.046% Mg.

Steel composition ranges between: 0.38 - 0.47% C; 0.52 - 0.82% Si; 0.4 - 0.7% Mn; 0.05 - 0.08% A1.

3. Experimental results

The experimental results are plotted in fig. 2 and 3 for spheroidal graphite cast iron and in fig. 4 for the aluminium alloy. In these figures, solidification time is related to the maximal temperature as recorded in the mould. Solidification start is taken as the time at which the metal enters the mould cavity and the thermocouple begins to deivate from the room temperature voltage. The time of maximal cooling rate recorded after the eutectic arrest is taken as the end of solidification. Interpolation in fig. 2-4 allows to calculate the solidification time for a specific maximal mould temperature. These data will then be used for subsequent analysis. As opposed to cast iron and the aluminium alloy which solidify as eutectics, the steel alloy solidifies over a temperature interval. This makes it difficult to accurately identify the end of solidification. More reliable results are obtained by directly comparing experimental and simulated cooling curves.

4. Simulation model

Simulation is used to compare the experimental data with a one-dimensional or a three-dimensional finite volume model of the sand coated die. The one-dimensional model calculates the frontal heat flow F from the centre of the casting to the die (Fig. 9). It is based on the implicit method for solving the discretized heat conduction equation. The three-dimensional model represents the experimental configuration as shown in fig. 1. For reasons of symmetry only one quarter of the casting and the mould

has to be modelled, corresponding to the top-right part in fig. 1, left. The three-dimensional model is based on a new developed alternating direction method. The details of this method have been published previoulsy [5-6].

All results are related to the solidification time in a pure sand mould. For this foundry application, one is indeed interested in the relative cooling rates and not in the absolute solidification times. Preliminary simulations showed that there was no influence of heat transport during mould filling on the relative solidification time. Hence simulation starts with a completely filled mould with metal at uniform temperature. During liquid cooling, natural convection creates a non-symmetric temperature distribution in the metal. However, previous research has shown that the difference between a model which takes natural convection into account and a stagnant liquid model gradually disappears towards the end of solidification [7]. Since the present results only require the total solidification time, natural convection can be neglected. The increased heat transport by convection is approximated by artificially enlarging the thermal conductivity of the liquid metal. Solidification is taken into account by enlarging the specific heat of the metal within the solidification interval. To this extent, a special function is applied which results in good agreement between experimental and simulated solidification morphology [8].

Thermal conductivity and specific heat are temperature dependent, densities are kept constant (Table 1). Moulding sand density is an experimental value at room temperature. Minor changes in the material properties have no influence on the simulated relative solidification time. Depending on the sand thickness, a maximum of 1458 elements were included in the three-dimensional model. A time step of 3 seconds for the complete ADI cycle was adopted. Variation of the time step between 0.75 s and 9 s and a reduction of the discretization form 5 mm to 2.5 mm in the sand layer did not change the relative simulation results.

Simulation results showed a substantial influence from the way the sand between casting and die is being discretized. A sand thickness of e g 20 mm can be discretized by 1 element measuring 20 mm or by 2 elements of 10 mm, or by 4 elements of 5 mm. Although the total sand thickness remains unchanged, the relative simulation results will vary considerably. Consequently, different sand thicknesses have been realized by varying the number of the elements while keeping their width constant at approximately 5 mm.

When comparing the experimental and simulation results it became obvious that no perfect conduction contact exist at the sand-die interface. Perfect conduction contact between elements [i, j] and [i+1, j] (Fig. 5) results in a heat transport rate Q_c between both elements:

$$Q_c = (T_{i+1,j} - T_{i,j})\ \Delta y_j \frac{2}{\frac{\Delta x_i}{k_i} + \frac{\Delta x_{1+1}}{k_{i+1}}} \tag{1}$$

T being the temperature and k the thermal conductivity. No perfect conduction contact has been implemented by reducing Q_c by a factor f, equalling the fraction of the interface contact area with perfect contact between both materials. On the remaining fraction of the area, (1−f), heat transport by radiation Q_r is taken into account. Heat conduction in the air is neglected. As a result, the heat transport rate Q between both elements becomes:

$$Q = Q_c \cdot f + Q_r \cdot (1-f) \tag{2}$$

$$Qr = \sigma \frac{1}{\frac{1}{\varepsilon_{i,j}} + \frac{1}{\varepsilon_{i+1,j}} - 1} (T^4_{i+1,j} - T^4_{i,j})\ \Delta y_j \tag{3}$$

with σ the Stefan-Boltzmann constant and ε the emittance.

TABLE 1 - Relevant Material Properties

MOULDING SAND

SPECIFIC HEAT [J/kg K] [11]

temperature T <= 760°C

$$c = -5.40\ 10^{-4}\ (T+273)^2 + 1{,}15\ (T+273) + 547.24$$

temperature T > 760°C

$$c = 1065{,}97 + 8.67\ 10^{-2}\ (T+273)$$

THERMAL CONDUCTIVITY [W/mK] [10]

$$k = -1.285\ 10^{-10}\ T^3 + 5.260\ 10^{-7}\ T^2 - 4.778\ 10^{-4}\ T + 0.873$$

THERMAL CONDUCTIVITY [W/mK] [11]

$$k = 1.758\ 10^{-7}\ (T+273)^2 - 1.676\ 10^{-4}\ (T+273) + 0.333$$

DENSITY [kg/m^3] = 1450

EMITTANCE 0.76

CAST METAL

DENSITY [kg/m^3]

7000 cast iron
6750 steel
2650 Al-Si

SPECIFIC HEAT [J/kg K] [11]

(spheroidal graphite cast iron)

$-0.04\ (T+273) + 974.92$ (T > 1200°C)
$1.71\ (T+273) - 1602.8$ (T: 1100-1200°C)
$0.14\ (T+273) + 556.23$ (T: 803-1100°C)
$0.59\ (T+273) + 69.93$ (T: 662- 803°C)
$0.13\ (T+273) + 497.04$ (T < 662°C)

(steel)

$0.21\ (T+273) + 354.34$

(Al-Si)

$0.46\ (T+273) + 766.17$ (T < 574°C)
1086 (liquid state)

THERMAL CONDUCTIVITY [W/m K]

(cast iron)

21.77 (solid state, T > 1000)
83.72 (liquid state)
$-0.0323\ (T+273) + 51.75$ (T < 443°C) [11]
$-0.0209\ (T+273) + 43.61$ (T > 443°C)

(steel)

$-0.18\ (T+273) + 349.99$ (T > 1495°C)
$0.0097\ (T+273) + 15.19$ (T: 809-1495°C)
154.61 (liquid state)

(segue)

(Al-Si)
142.3 (solid state)
211.27 (liquid state) [12]

SOLIDIFICATION INTERVAL [°C]

1156-1078 (cast iron)
1492-1442 (steel)
574- 547 (Al-Si)

LATENT HEAT OF FUSION [kJ/kg]

(Cast Iron) 259.6
(Steel) 277
(Al-Si) 561.7

Within the solidification interval the specific heat is increased with:

$$\text{for steel and Al-Si: } \frac{L}{T_s - T_e}$$

where L is the latent heat of fusion, T_s and T_e the start and final temperature of solidification resp.

For spheroidal graphite cast iron [8]:

$$23.6\ \frac{L}{T_s - T_e}\left(\frac{1}{R_f - (R_f - R_i)\,x} - \frac{1}{R_f}\right);\ x = \frac{T - T_e}{T_s - T_e}$$

with R_f (R_i) the final (initial) austenite shell thickness;

$R_f/R_i = 4$; $R_f = 20$ μm and $R_i = 5$ μm.

DIE

DENSITY [kg/m^3] 7250

SPECIFIC HEAT [J/kg K] [11]
0,133 (T+273) + 497.04 (T<662°C)
0,59 (T+273) + 69.93 (T: 662- 803°C)
0,138 (T+273) + 556.23 (T: 803-1100°C)

THERMAL CONDUCTIVITY [W/m K] [11]
−0,104 (T+273) + 108.09 (T<662°C)
−0,03 (T+273) + 61.55 (T: 328-717°C)
−0,072 (T+273) + 106.27 (T>717°C)

HEAT TRANSFER COEFFICIENT [W/K m^2] [7]

FREE CONVECTION IN THE AIR (HORIZONTAL)

$$(4.517\ 10^{-7}\ T^2 - 1.070\ 10^{-3}\ T + 1.627)\ (T - T_{air})^{0.33}$$

FREE CONVECTION IN THE AIR (VERTICAL) [13]
$2.164\ (T - T_{air})^{0.25}$ (T<360°C)
$(2.270 - 2.94\ 10^{-4}\ T)\ (T - T_{air})^{0.25}$ (T: 360 − 700°C)
$(2.371 - 4.38\ 10^{-4}\ T)\ (T - T_{air})^{0.25}$ (T: 700 − 1000°C)

EMITTANCE 0.88

5. Simulation results

Comparison between experimental and simulation results allows to estimate the value of f, the fraction of the area with perfect conduction contact between sand and die, at 0.3. This value does not depend on the metal being poured. Results are represented in Fig. 6, 7 for cast iron with casting thickness of 20 and 30 mm resp and in Fig. 8 for the 30 mm thick aluminium casting. Fig. 6 and 7 are plotted for an initial cast iron temperature of 1300°C and Fig. 8 for an aluminium temperature of 600°C. In the figures, simulation results are marked by a (+), curves in between are based on cubic splines interpolation.

The solidification in the centre of the 20 mm plate accords to a one-dimensional heat flow (Fig. 6). However, the 30 mm thick spheroidal graphite casting represents a three dimensional heat flow problem. The solidification time of the 30 mm casting is indeed influenced by the chilling effect of the die located at the side walls of the casting. It is shown schematically by the lateral heat flow L in Fig. 9. This explains the difference in solidification time recorded in a pure sand mould and in the sand coated die with a sand layer thick enough to eliminate the influence of the die parallel to the casting. Fig. 9 represents a cross-section of the sand coated die; lateral and frontal heat flow are labelled L and F. According to Boenisch et al [9], mould wall movement could deform the mould cavity as shown in Fig. 9 by the dashed line. Taking into account that aluminium shrinks during solidification, an air gap will form at the side wall which will considerably reduce the lateral heat flow L. The inward motion of the sand at the front and back planes of the casting will counteract or reduce the air gap formation. Consequently, the frontal heat flow F will be less influenced than the lateral one L. Contrary to aluminium alloys, spheroidal graphite cast iron expands during solidification resulting in relatively high forces on the mould wall. For this alloy, air gap formation may be excluded.

As stated higher, it is difficult to accurately deduce the end of solidification from the cooling curves of the steel castings. Fig. 10 compares experimental and simulated cooling curves recorded in the centre of the 20 mm thick casting. The good agreement validates the simulation model for steel.

The influence of the thermal conductivity of the moulding sand was evaluated by comparing simulation results based on conductivity data published by Kubo [10] and Pehlke [11]. Despite the considerable difference between both (Fig. 11), the influence on the relative simulation results as shown in Fig. 6-8, can be neglected.

6. Literature comparison

6.1 Böhm's Result for Steel [2]

Böhm has published results for square plate castings with thickness of 50, 100 and 300 mm. Because the width of the castings equals 5 times the thickness, the cooling in the centre may be approximated by a one-dimensional model. Castings were poured horizontally. The die thickness equals 10 or 40 mm. Results of all combinations are compiled in figures 12-16. Experimental data as well as simulation results are related to the solidification time in a pure sand mould. At the die-air interface, the formulas which govern heat transport by free convection differ for a vertical or a horizontal mould (Table 1). However, simulation results were identical for either of both.

Simulation results fit experiment very good when the die is relatively thick as compared to the casting (Fig. 12, 14). In these circumstances, the die can absorb the latent heat of fusion of the casting without reaching quickly, a steady, high temperature at the outer side, sc at the die-air interface (Fig. 17).

When the ratio of casting thickness to die thickness increases, the die cannot absorb the liberated heat. A high temperature is established at the outer die surface where the heat is transferred by convection and radiation. It is illustrated in Fig. 17 for the 300 mm casting. The simulation model is based on a free surface die-air. Since the experimental castings of Böhm are very large, the horizontal bottom surface was probably resting on the floor. IN this configuration, heat transfer at the bottom plate is governed by conduction which is smaller than the radiative heat transfer at higher temperatures (e g 600°C). As a result, the total cooling rate decreases and the experimental solidification time will shift towards the one recorded in a pure sand mould. This is reflected in Fig. 15 and 16 in Fig. 13 for an intermediate case. Hence, the discrepancy between simulation and experiment in the last figures is most likely not attributed to a bad simulation model but resulting from a large difference between the experimental configuration and the simulated configuration.

6.2 Schürmann's Result for Cast Iron [3]

Schürmann experimented with a pure 3.5% Carbon-Iron alloy in a sand coated die configuration which is very similar to one used in the present investigation. Sand thickness ranges between 2 and 10 mm for a casting thickness between 3 and 19 mm. Based on his experiments, Schürmann derived a formula for the solidification time t_s in a sand coated die [dimension s]:

$$t_s = 0.28\ 10^4 \frac{D^{1/2}}{T_B - T_F} M + 0.79\ 10^3 \frac{D^{1/2}}{T_B - T_F} M^2 \qquad (4)$$

where D is the sand thickness [mm], M the casting modulus [mm], T_B the interface temperature casting-sand [1070°C] and T_F the mould temperature prior to casting [20°C]. Schürmann's formula has been plotted in figure 18 for a plate casting of 15 mm thickness (modulus 7.5 mm). The same figure shows the results of a one-dimensional simulation for cast iron. For an initial metal temperature of 1250°C, Schürmann's formula and the simulation both predict a solidification time of 139 s in a 5 mm thick sand coated die.

Examination of figure 18 reveals a perfect coincidence for send thicknesses between 2 and 13 mm, covering the range of Schürmann experiments. However outside this interval erroneous results are predicted by equation (4). When the sand thickness goes to zero, so dose the solidification time while the latter grows unboundedly with increasing sand thicknesses. It is obvious that both conditions are physically impossible.

7. Sand-die interface

The heat transfer model at the sand-die interface is based on a perfect conduction contact area fraction f of 0.3 and a radiative heat transfer on the remaining area fraction. The previous results show that this simulation model is in good agreement with the experimental data of different origin. The reduced conduction at the interface could be caused by the formation of an air gap at about 30 percent of the interface. However, it would be astonishing to find this value in three different experiments. Moreover, two experiments (the present and Schürmann's one) use a vertical interface while Böhm experimented with horizontal castings. This suggests that there could be a more fundamental explication for the "constant" value of f equalling 0.3.

7.1 A Simplified Model

Fig. 19 shows a simplified model of sand grains in the vicinity of the sand-die interface. In this model all grains are of the same diameter R and are close-packed in space. Temperature isotherms are supposed to be parallel to the interface producing heat flow in the direction u in Fig. 19. Conductive heat transport between the grains E and G may be approximated as:

along EZG: $\frac{\varepsilon\ \Delta T}{2R}$; $\Delta T = T_E - T_G$

along EXYG: $\frac{\varepsilon\ \Delta T}{3R}$

where ε is the contact area between two grains.

$$\text{Total} = 1\ (EZG) + 4\ (EXYG) = \varepsilon\ \Delta T\ (\frac{1}{2R} + \frac{4}{3R}) = \frac{11}{3}\ (EZG)$$

In the close-packed structure only 1 row grains of two touches the die which result in a ratio of conductive heat transport at the sand-die interface versus conductive heat transport in the sand π of:

$$\tau_p = \frac{1/2\ (EZG)}{11/3\ (EZG)} = \frac{3}{22} = 0.136 \qquad (5)$$

Six grains are involved to transfer heat from grains E to G, giving 5 conduction paths. In a non-perfect packing, grains may be missing. A missing grain in the sand reduces the conduction heat transfer by 1/5; at the sand-die interface it will decrease by 1/6. This allow to correct the value of π:

$$\text{1 grain missing:} \quad \tau = \tau_p \frac{5/6}{4/5} = 0.284 \qquad (5A)$$

$$\text{2 grains missing:} \quad \tau = \tau_P \frac{4/6}{3/5} = 0.303 \qquad (5B)$$

Finally it should be mentioned that moulding sand is composed of different grain sizes. This will decrease the number of contact points between the grains as compared to a closest packing where it is maximal. This effect will be much lower at the sand-die interface.

7.2 Experimental Facts

Experiments were carried out with AFS 75 silica sand. The different grain sizes within the sand are illustrated in Fig. 20. For pure dry sand, the fraction of solid has been measured experimentally, giving 0.55. A hexagonal closest packing shows as solid fraction:

0.74 (perfect)
0.62 (1 grain missing per unit cell)
0.49 (2 grains missing per unit cell)

These figures show, for the simplified model represented in figure 19, that about 1.55 grains are missing per unit cell in the experimental sand. Comparing this value with the figures listed previously as (5A, B), a value for π of 0.29 results which is very close to the experimental value of 0.3 for f, representing the fraction of the ara at the sand-die interface with perfect conduction contact.

8. Conclusion

The sand coated die allows to decrease the solidification time by reducing the sand thickness between casting and die. However, the range of sand thicknesses which allow to influence the casting solidification time is rather small. A solidification time below 50 percent of the one recorded in a pure sand mould is only achievable with sand thicknesses which are about 1 order of magnitude lower than the casting thickness. When the sand thickness equals the casting thickness, the chilling influence of the die becomes negligible.

A computer model has been developed which accurately predicts the relative solidification time in the sand coated die. This model, validated for several cast metals, is in close agreement with the experimental data of the present research as well as with the ones published previously in literature. Changes in material property data alter the absolute simulation results, however the relative solidification time which is related to the one in a pure sand mould, is not influenced.

It has been shown that the perfect conduction contact area fraction at the interface sand-die equals about 30 percent. This value can be explained by a simplified model of sand grains packing. It originates from the lower number of conduction contact points at the sand-die interface as compared to the sand itself.

It is difficult to plot graphs which generalize the present results for practical applications since the number of process variables is much to high. These include casting, sand and die thickness, initial metal and die temperature, and the type of metal casted. Acceptable results for any combination may be obtained by a simple one-dimensional simulation model. Essential in this model are the material properties which are listed in Table 1. For completeness, the basic equations building the numerical model are derived in the appendix.

Appendix

Although the basic equations which build a simulation model may be found in standard books on heat transfer [14], they are derived here for completeness. The equations are given for a one-dimensional heat transfer model (figure 21). As shown in the article, such a simplified model allows to accurately calculate the solidification behaviour in the sand coated die.

The temperature change of element [i] (equation A1, left hand side) may be calculated by evaluating heat transport to or from the surrounding elements [i−1] and [i+1] (equation A1, right hand side):

$$\Delta x_i \; d_i \; c_i \frac{T_i^{n+1} - T_i^n}{\Delta t} = \frac{T_{i-1}^{n+1} - T_i^{n+1}}{\frac{\Delta x_i}{2k_i} + \frac{\Delta x_{i-1}}{2k_{i-1}}} + \frac{T_{i+1}^{n+1} - T_i^{n+1}}{\frac{\Delta x_i}{2k_i} + \frac{\Delta x_{i+1}}{2k_{i-1}}} \qquad \text{(A1)}$$

where d is the density, c is the specific heat, T is the temperature, t is the time and k the thermal conductivity. Indices i and n represent the discretization with respect to space and time resp. Rearranging

equation (A1) gives equation (A2) which expresses the unknown temperatures at the next time level as a function of the known temperatures at the previous time level.

$$A_i\ T_{i-1}^{n+1} + B_i\ T_i^{n+1} + C_i\ T_{i+1}^{n+1} = T_i^n \tag{A2}$$

with

$$A_i = -\frac{\Delta t}{c_i\ d_i\ \Delta x_i}\ \frac{1}{\frac{\Delta x_i}{2k_i} + \frac{\Delta x_{i-1}}{2k_{i-1}}} \tag{A3}$$

$$C_i = -\frac{\Delta t}{c_i\ d_i\ \Delta x_i}\ \frac{1}{\frac{\Delta x_i}{2k_i} + \frac{\Delta x_{i+1}}{2k_{i+1}}} \tag{A4}$$

$$B_1 = 1 - A_i - C_i \tag{A5}$$

Repeating this procedure for all elements results in the tridiagonal system (A6). A very efficient procedure known as the Thomas algorithm, exists to solve this kind of system. It may be found in all standard books on numerical methods [15].

$$B_1\ T_1^{n+1} + C_1\ T_2^{n+1} = T_1^n$$

$$A_i\ T_{i-1}^{n+1} + B_i\ T_i^{n+1} + C_i\ T_{i+1}^{n+1} = T_1^n \tag{A6}$$

$$A_m\ T_{m-1}^{n+1} + B_m\ T_m^{n+1} = T_m^n$$

The proceeding procedure is known as the implicit method which is unconditionally stable. An alternative is to adopt the explicit method which allows to calculate the new element temperature directly (equation A7). However this method limits the time step (equation A8).

$$T_i^{n+1} = A_i'\ T_{i-1}^n + (1 - A_i' - C_i')\ T_i^n + C_i'\ T_{i+1}^n \tag{A7}$$

$$A_i' = -A_i > 0;\ C_i' = -C_i > 0$$

$$1 - A_i' - C_i' >= 0 \tag{A8}$$

For element [1], located at a symmetry plane, A_1 in equation (A2) equals 0. The heat balance for the last element [m], which exchanges heat by radiation and convection of the air, is given in equation (A9).

$$\Delta x_m\ d_m\ c_m\ \frac{T_m^{n+1} - T_m^n}{\Delta t} = \frac{T_{m-1}^{n+1} - T_m^{n+1}}{\frac{\Delta x_m}{2k_m} + \frac{\Delta x_{m-1}}{2k_{m-1}}} + h\ (T_{air} - T_m^{n+1}) \tag{A9}$$

where h is the heat transfer coefficient. Rearranging gives equations (A10, A11).

$$A_m\ T_{m-1}^{n+1} + B_m^*\ T_m^{n+1} = T_m^n + \frac{h\ \Delta t}{\Delta x_m\ d_m\ c_m}\ T_{air} \tag{A10}$$

with

$$B_m^* = 1 - A_m + \frac{h\ \Delta t}{\Delta x_m\ d_m\ c_m} \tag{A11}$$

At the interface sand-die, imperfect conduction contact has to be taken into account. If the interface is located between elements [i] and [i+1], some corrections are necessary.

$$A_i\ T_{i-1}^{n+1} + B_i\ T_i^{n+1} + C_i^*\ T_{i+1}^{n+1} = T_i^n \tag{A12}$$

$$B_i = 1 - A_i - C_i^* \tag{A13}$$

$$C_i^* = f C_i - (1-f)\frac{\Delta t}{\Delta x_i\ d_i\ c_i} h_{rad} \tag{A14}$$

$$h_{rad} = \sigma \frac{1}{\frac{1}{\varepsilon_i} + \frac{1}{\varepsilon_{i+1}} - 1} (T_{i+1}^2 + T_i^2)\ (T_{i+1} + T_i) \tag{A15}$$

In equation (A15) temperatures are expressed in kelvin, the other symbols have the same meaning as in equation (3). Similar corrections are needed when making the heat balances for element [i+1], be it that the coefficient A has to be modified in stead of C.

References

[1] Snezhnoi, R.L., W.S. Serebro, J.M. Rywkis and B.W. Rabinowitsch. *Technologische Grundlagen und komplexe Mechanisierung der Herstellung von Gußstücken aus Eisenmetallen in ausgekleideten Kokillen*. 40th Int. Foundry Congress (1973), 14;

[2] Böhm, H.J. *Steuerung der Erstarrung bei Stahlguß durch Kühl- und Isolierelemente unter Sand.* Giesserei, 63 (1976), 501-506;

[3] Schürmann, E. and W. Dohmen. *Messung der Erstarrunsgeschwindigkeit von Gußeisen in sandbeschichteten Kokillen und die Entwicklung einer zugehörigen Erstarrungsgleichung.* Giesserei, 59 (1972), 569 -576;

[4] Schürmann, E. and H. Löblich. *Einfluß der Maskendicke einer sandbeschichteten Kokille auf Erstarrungsgeschwindigkeit,* Graphitausbildung und Härte von Gußeisen. Giess.-Forsch., 27 (1975), 95-101;

[5] Mampaey, F. *A Numerical Technique to Increase the Stability of the ADI method in Solidification Simulation.* J. Computational and Applied Math., 28 (1989), 297-308;

[6] Mampaey, F. *A stable alternating direction method for simulating three-dimensional solidification problems.* In Lewis, Morgan (Ed.), *Numerical Methods in Thermal Problems,* Pineridge Press, Swansea U.K., 1989, vol. VI, pp. 1174-1184;

[7] Mampaey, F. *Study of natural convection in castings.* 56th World Foundry Congress Düsseldorf (1989) Paper 10;

[8] Mampaey, F. *Numerical Simulation of the Solidificatoin Morphology of Cast Iron.* Proc. FOCOMP Conf. KRAKOW POLAND, 1986 pp. 74-90;

[9] Boenisch, D., S. Engler and B. Köhler. *Einfluß von Formstroff und Gießtemperatur auf bewegung und Ausdehnungsdruck der Formwand.* Giesserei, 60 (1973), 669-681;
[10] Kubo, K., K. Mizuukchi, I. Ohnaka and T. Fukusako. *Measurement of Thermal Properties of Sand Molds by Pouring Method.* 50th World Foundry Congress Cairo (1983) Paper 6;
[11] Pehlke, R.D., A. Jeyarajan and H. Wada. *Summary of Thermal Properties for Casting Alloys and Mould Materials Nat. Science Found.*, Washington, 1982;
[12] Smithells, C.J. *Metals Reference Book,* Butterworths, London, 1967;
[13] VDI-Wärmeatlas. *VID-Verlag,* Düsseldorf, 1963;
[14] Shih, T.M. *Numerical Heat Transfer,* Hemisphere, Washington DC, 1984;
[15] Press, W.H., B.P. Flannery, S.A. Teukolsky and W.T. Vetterling. *Numerical Recipes,* Cambridge Univ. Press, 1987.

Figure legends

Fig. 1: Cross-sections of the sand coated die (dimensions in mm).

Fig. 2: Experimental solidification time as a function of maximal mould temperature for spheroidal graphite iron castings of 20 mm thickness. Figure legend identifies sand thickness; FSM Full Sand Mould.

Fig. 3: Experimental solidification time for spheroidal graphite iron castings of 30 mm thickness.

Fig. 4: Experimental solidification time for aluminium-silicon castings of 30 mm thickness.

Fig. 5: Schematic representation of adjacent elements.

Fig. 6: Solidification time in the sand coated die. Spheroidal graphite cast iron, casting thickness 20 mm.

Fig. 7: Solidification time in the sand coated die. Spheroidal graphite cast iron, casting thickness 30 mm.

Fig. 8: Solidification time in the sand coated die. Aluminium, casting thickness 30 mm.

Fig. 9: Schematic representation of heat flow and mould wall displacement (dotted line).

Fig. 10: Cooling curves for steel in the sand coated die for two sand thicknesses.

Fig. 11: Thermal conductivity for moulding sand according to Kubo [10] and Pehlke [11].

Fig. 12 to 16: Comparison between simulated and experimental results of Böhm [2].

Fig. 17: Simulated temperature at the outer die surface during solidification (Figures on the right give casting and die thickness in mm resp).

Fig. 18: Solidification time obtained by Schürmann's formula [3] and by the present simulation model.

Fig. 19: Closest packing of sand grains.

Fig. 20: Grain size distribution of the moulding sand (AFS 71).

Fig. 21: One-dimensional element ordering.

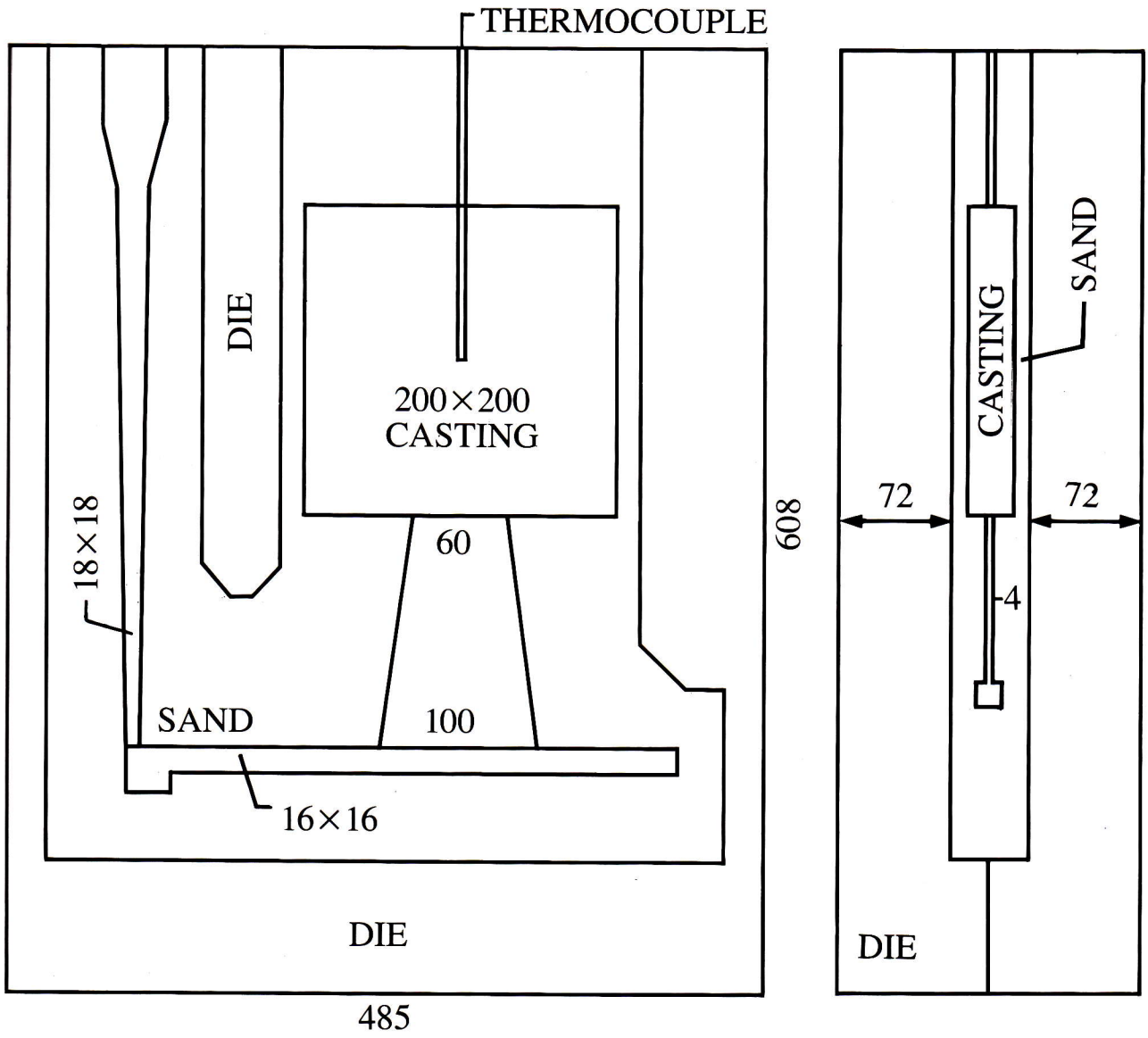
THERMOCOUPLE
DIE
200×200
CASTING
18×18
60
608
SAND
100
16×16
DIE
485
CASTING
SAND
72
72
4
DIE

Fig. 1

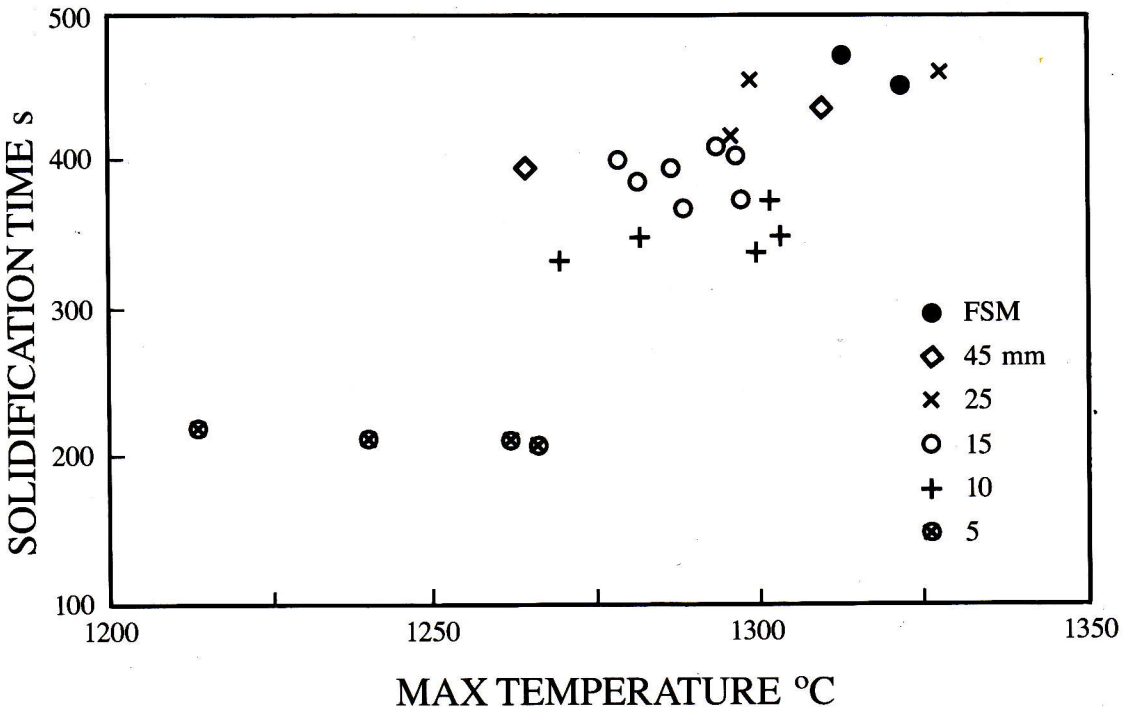
SOLIDIFICATION TIME s
500
400
300
200
100
1200
1250
1300
1350
MAX TEMPERATURE °C
FSM
45 mm
25
15
10
5

Fig. 2

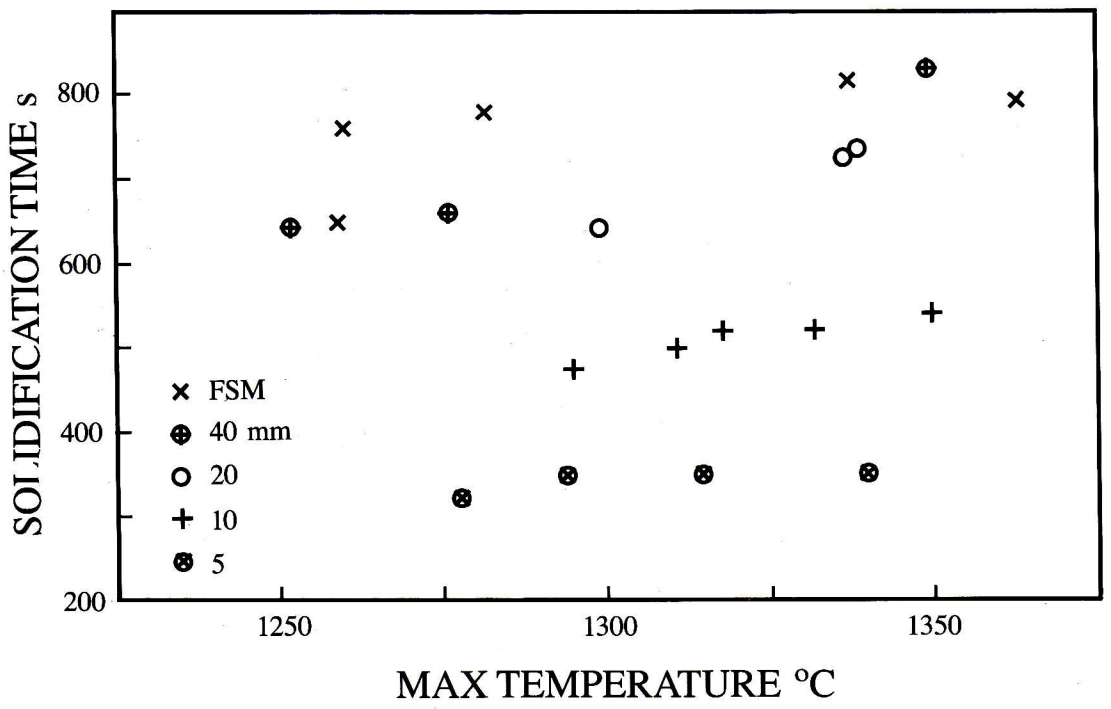
SOLIDIFICATION TIME s
800
600
400
200
1250
1300
1350
MAX TEMPERATURE °C
FSM
40 mm
20
10
5

Fig. 3

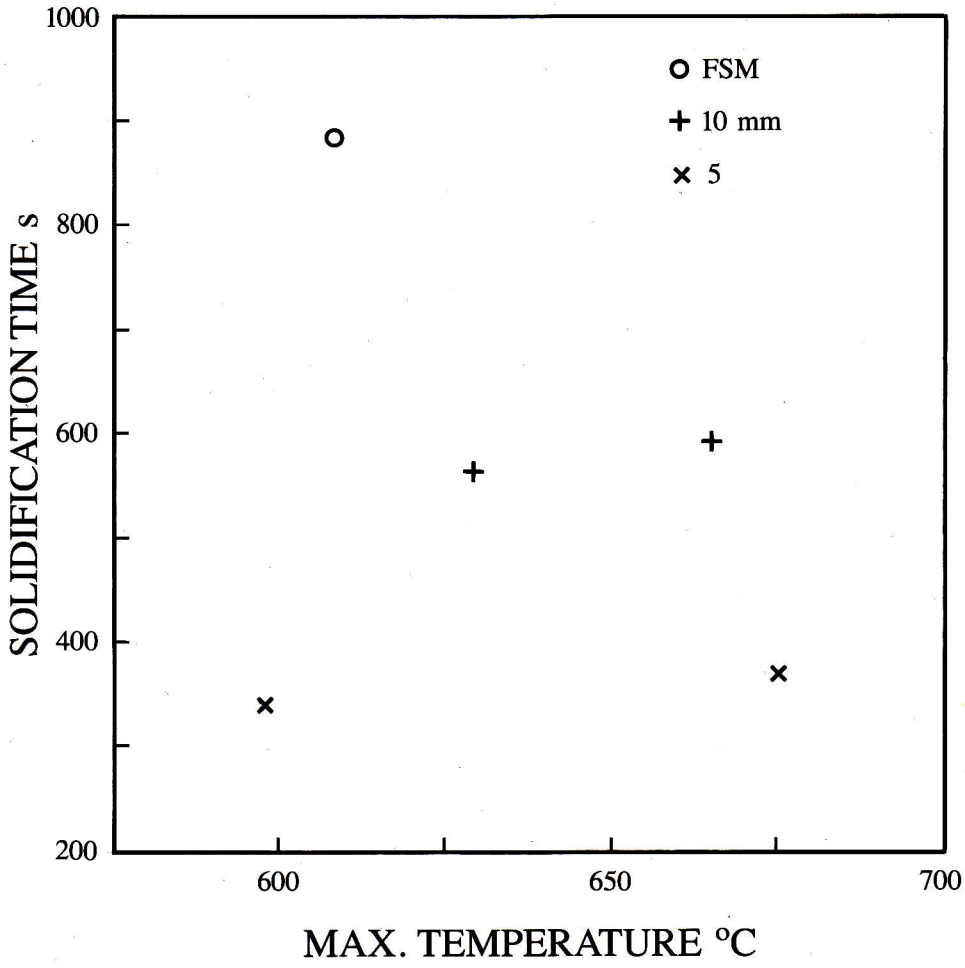
1000
800
600
400
200
SOLIDIFICATION TIME s
600
650
700
MAX. TEMPERATURE °C
FSM
10 mm
5

Fig. 4

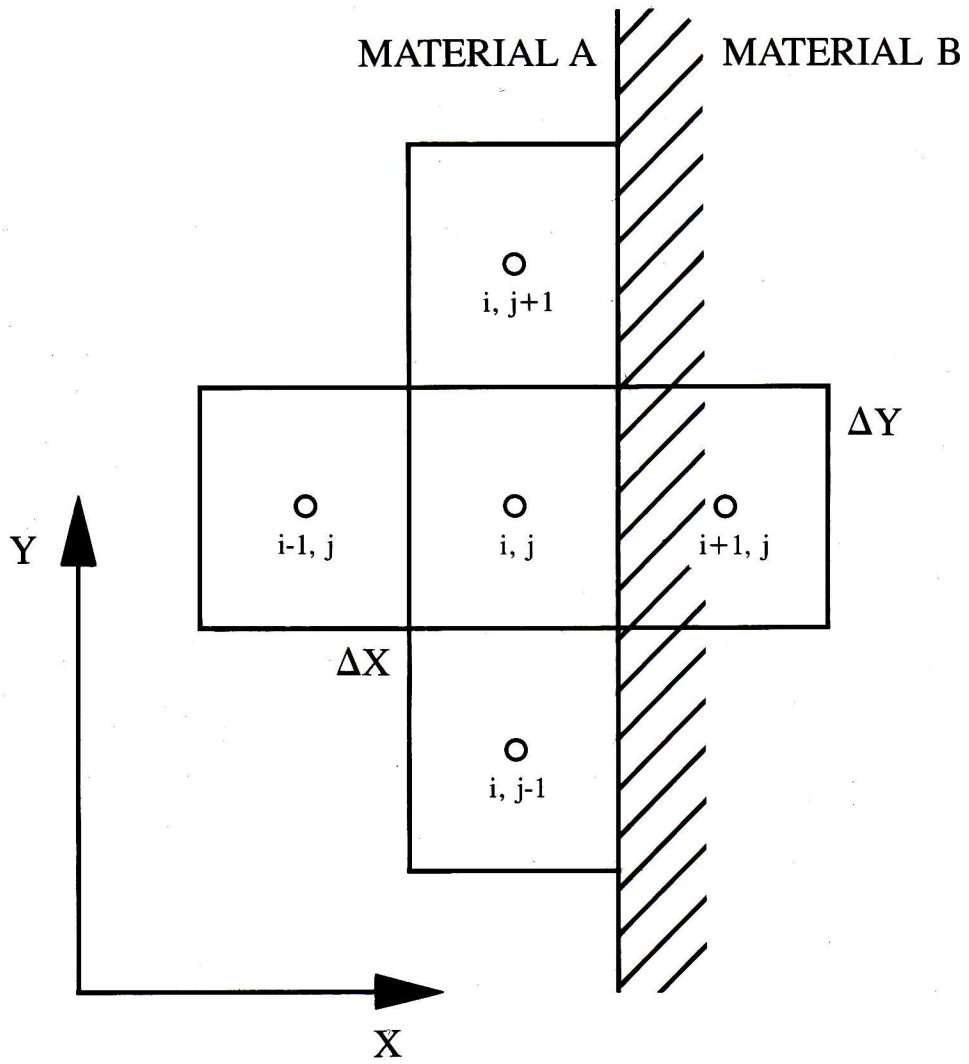

Fig. 5

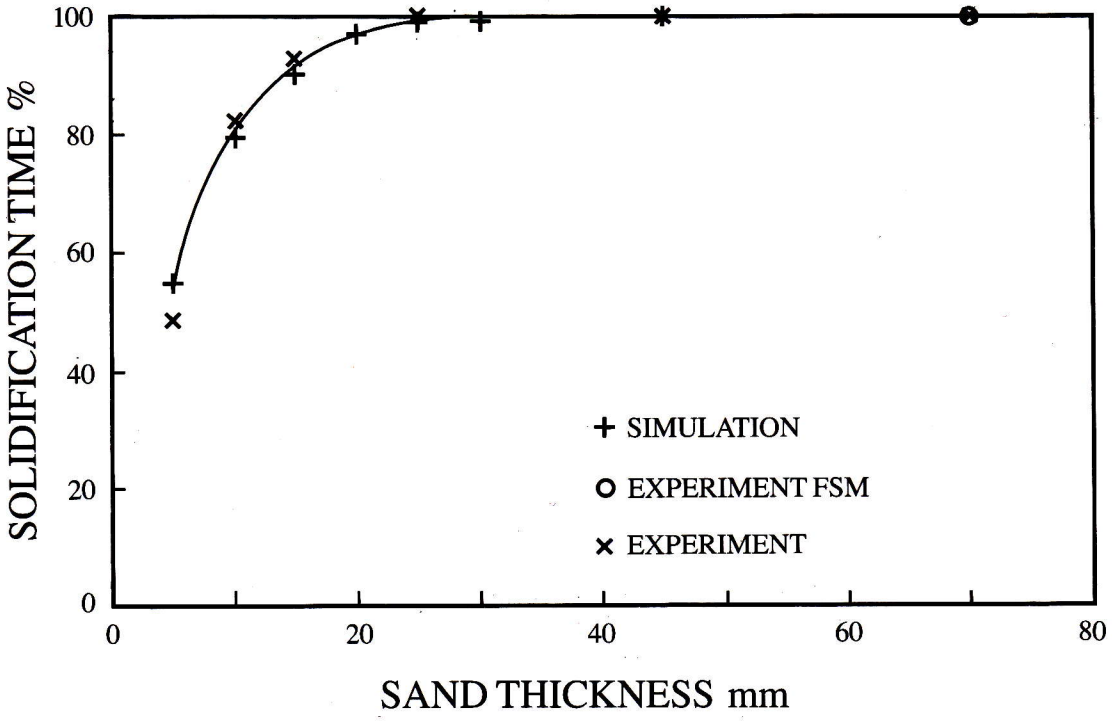
SOLIDIFICATION TIME %
100
80
60
40
20
0
0
20
40
60
80
SAND THICKNESS mm
+ SIMULATION
O EXPERIMENT FSM
× EXPERIMENT

Fig. 6

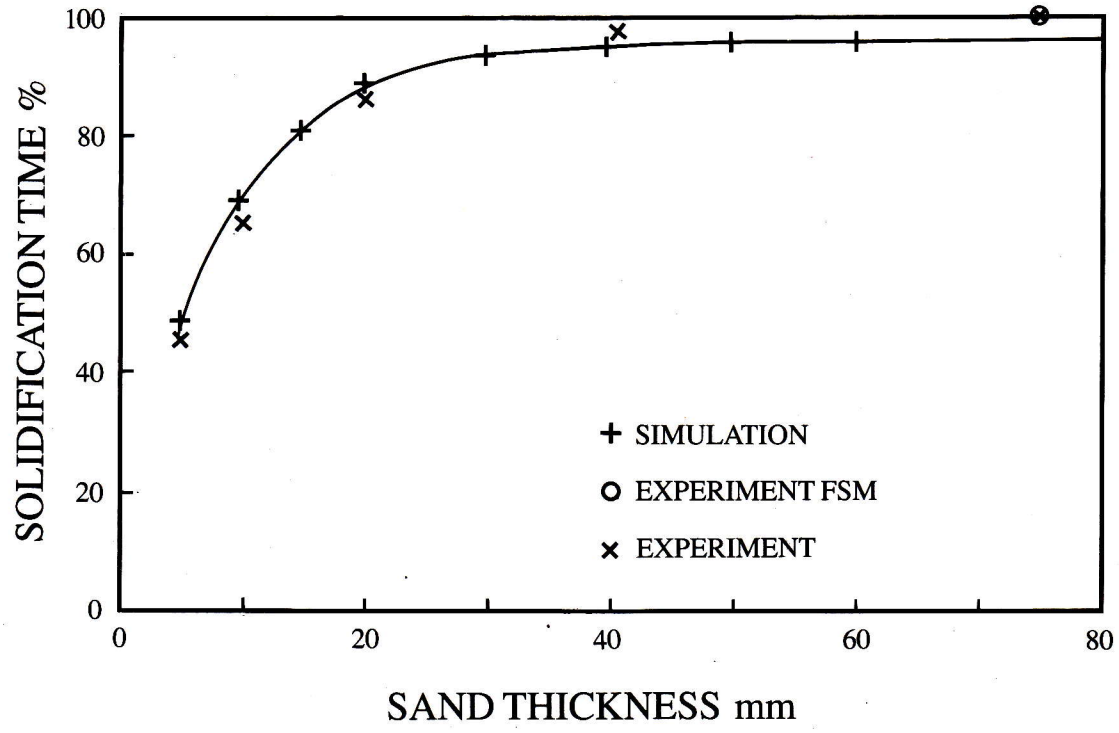
SOLIDIFICATION TIME %
100
80
60
40
20
0
0
20
40
60
80
SAND THICKNESS mm
+ SIMULATION
O EXPERIMENT FSM
× EXPERIMENT

Fig. 7

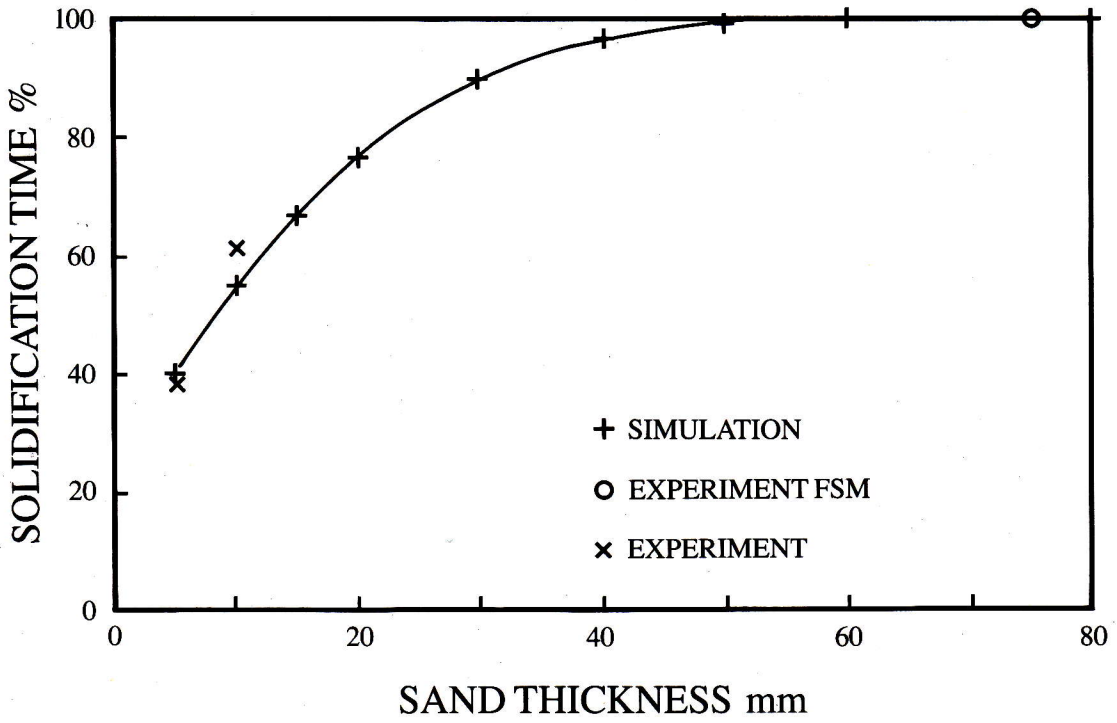
SOLIDIFICATION TIME %
100
80
60
40
20
0
0
20
40
60
80
SAND THICKNESS mm
+ SIMULATION
O EXPERIMENT FSM
× EXPERIMENT

Fig. 8

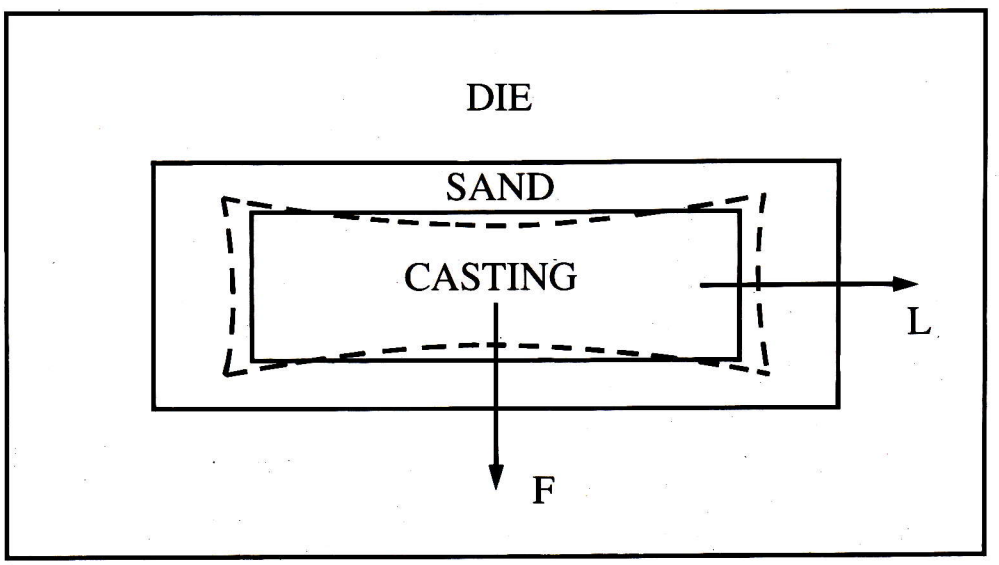
DIE
SAND
CASTING
L
F

Fig. 9

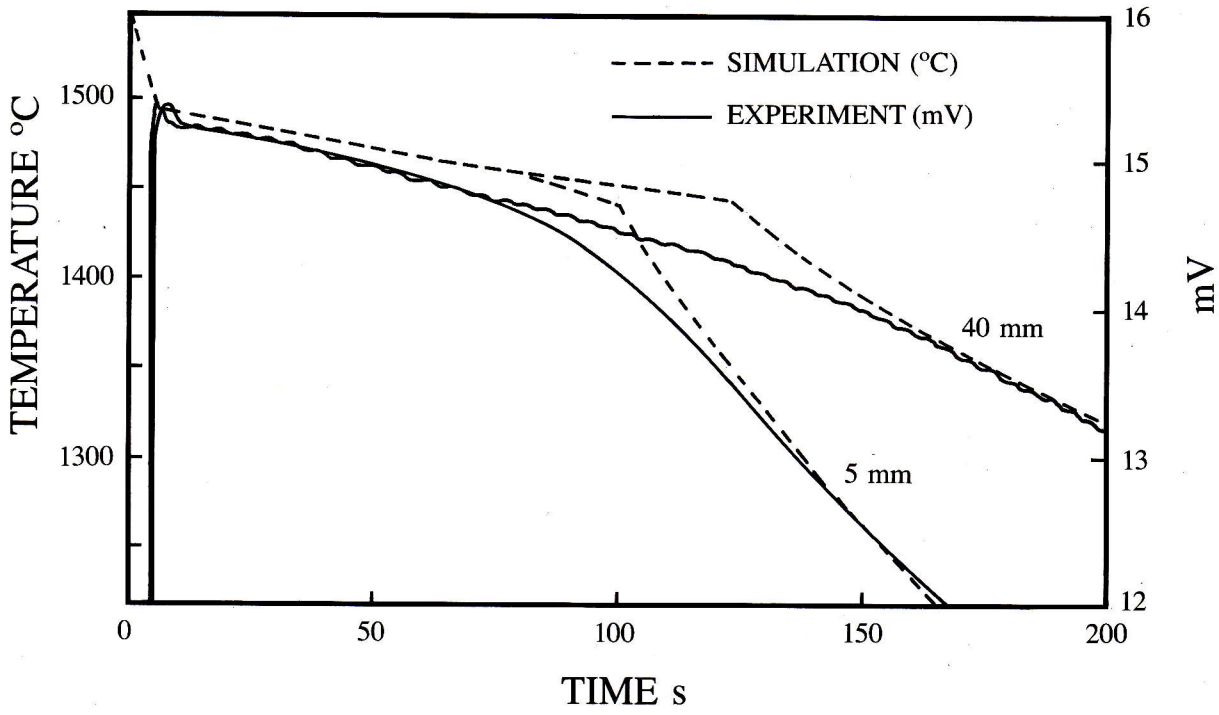
SIMULATION (°C)
EXPERIMENT (mV)
TEMPERATURE °C
mV
TIME s
40 mm
5 mm
1500
1400
1300
16
15
14
13
12
0
50
100
150
200

Fig. 10

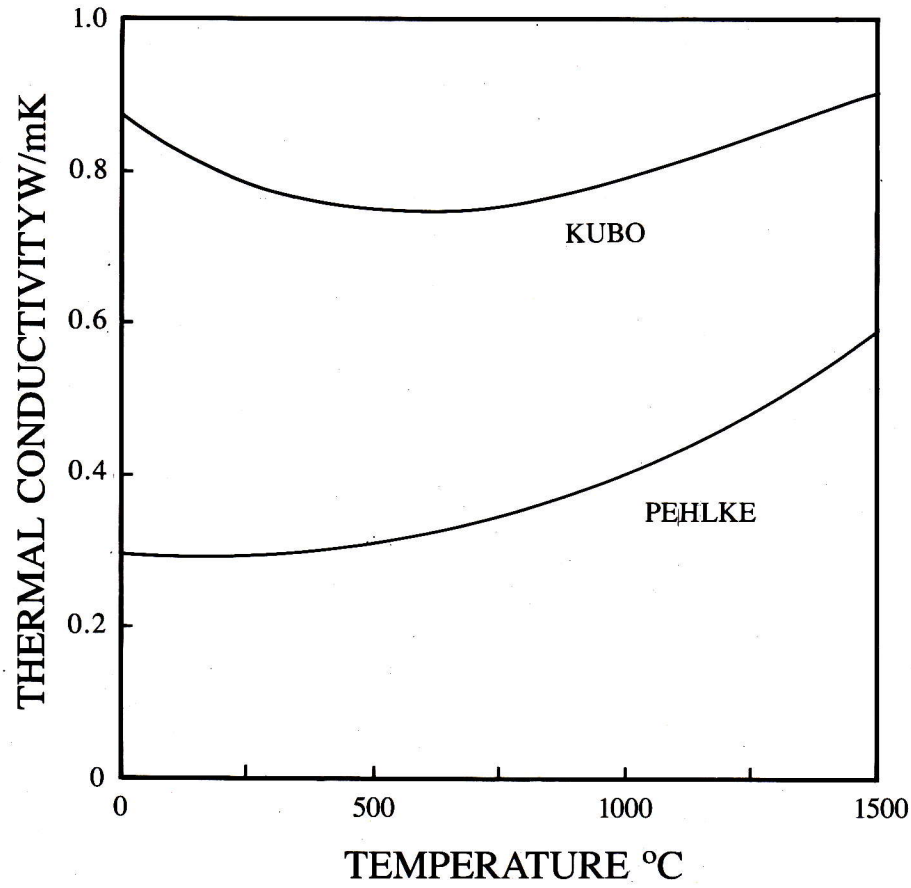
THERMAL CONDUCTIVITYW/mK
TEMPERATURE °C
KUBO
PEHLKE
1.0
0.8
0.6
0.4
0.2
0
0
500
1000
1500

Fig. 11

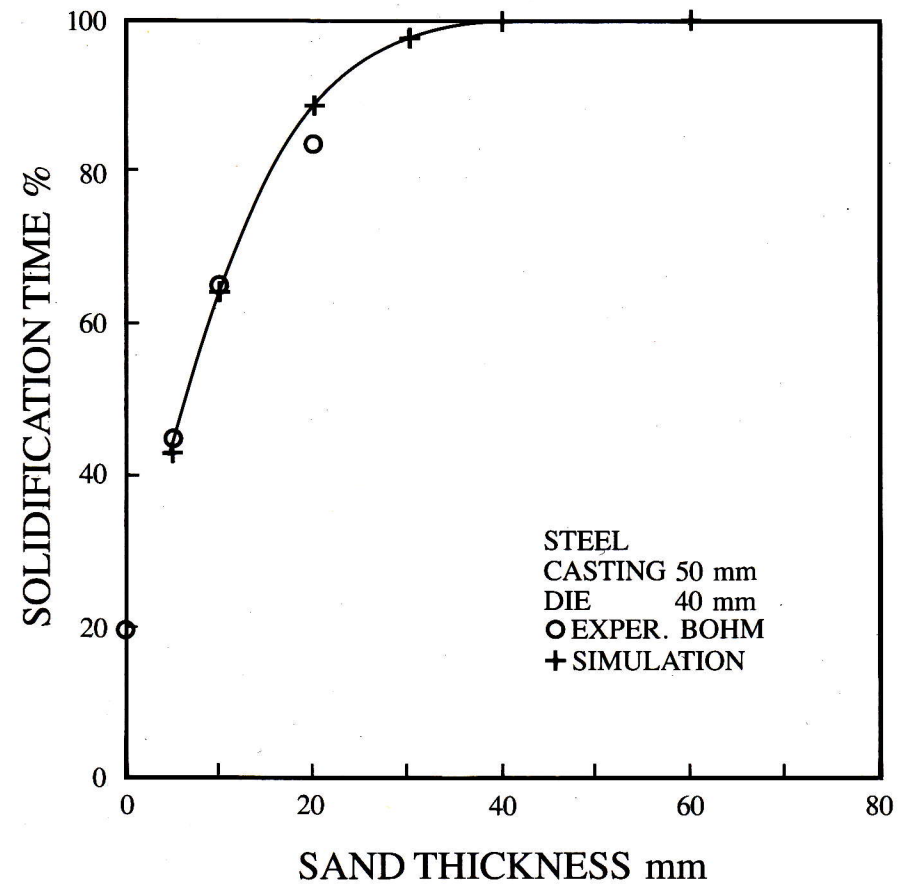
SOLIDIFICATION TIME %
100
80
60
40
20
0
0
20
40
60
80
SAND THICKNESS mm
STEEL
CASTING 50 mm
DIE 40 mm
O EXPER. BOHM
+ SIMULATION

Fig. 12

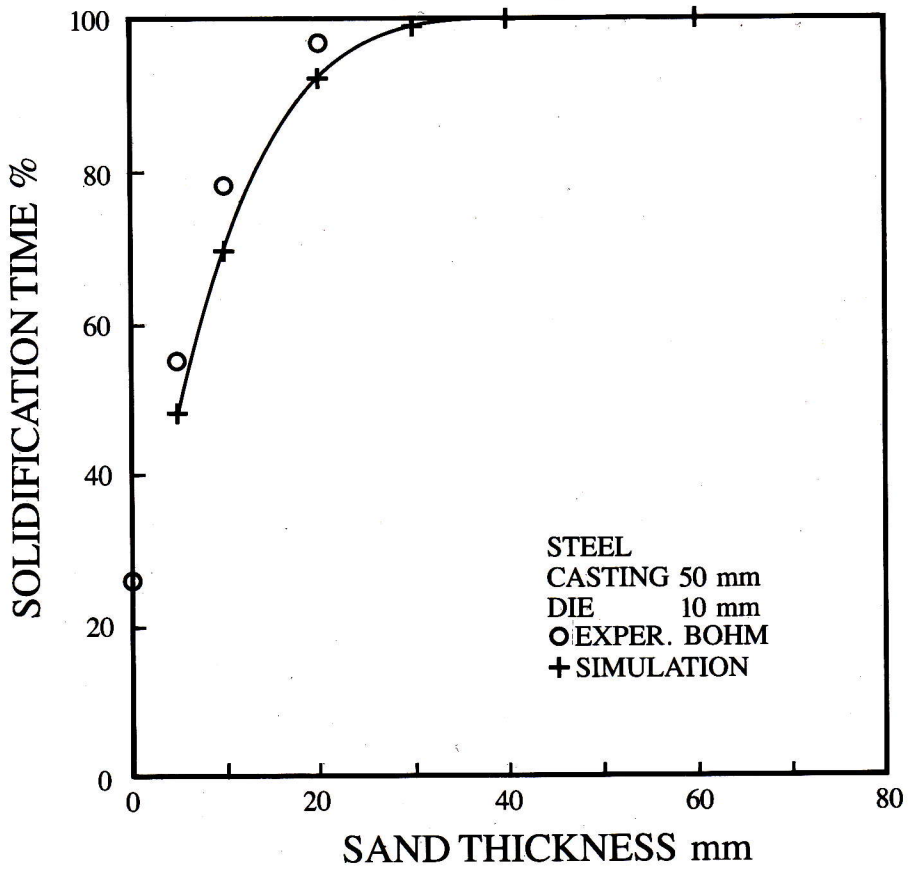
SOLIDIFICATION TIME %
100
80
60
40
20
0
0
20
40
60
80
SAND THICKNESS mm
STEEL
CASTING 50 mm
DIE 10 mm
O EXPER. BOHM
+ SIMULATION

Fig. 13

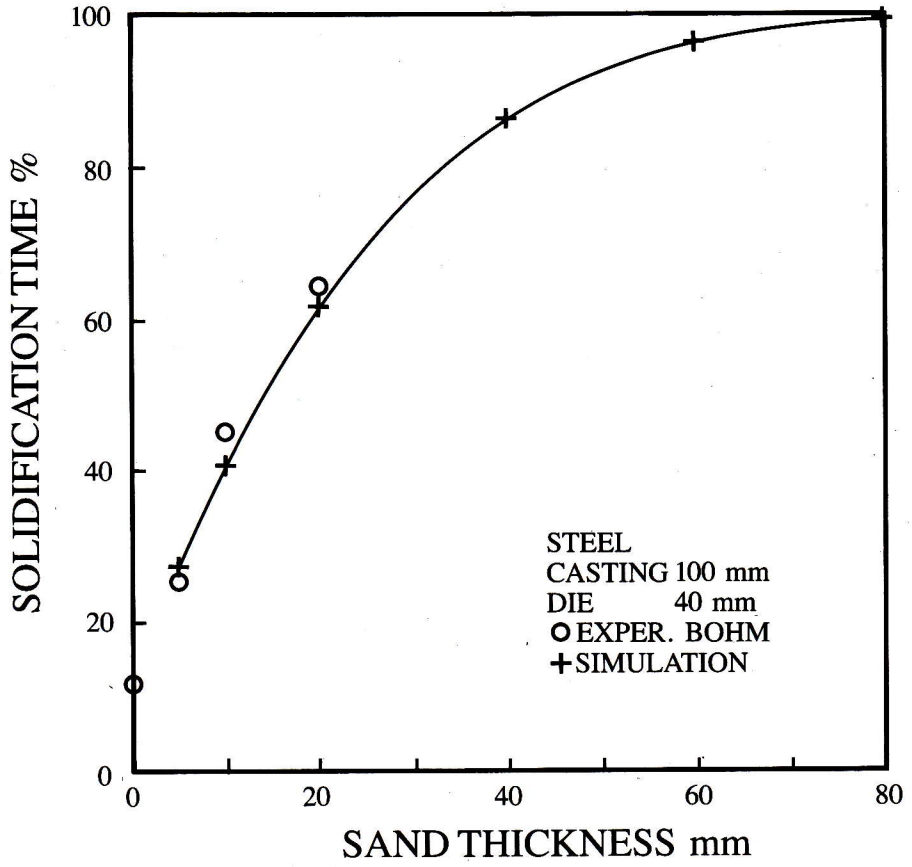
SOLIDIFICATION TIME %
100
80
60
40
20
0
0
20
40
60
80
SAND THICKNESS mm
STEEL
CASTING 100 mm
DIE 40 mm
O EXPER. BOHM
+ SIMULATION

Fig. 14

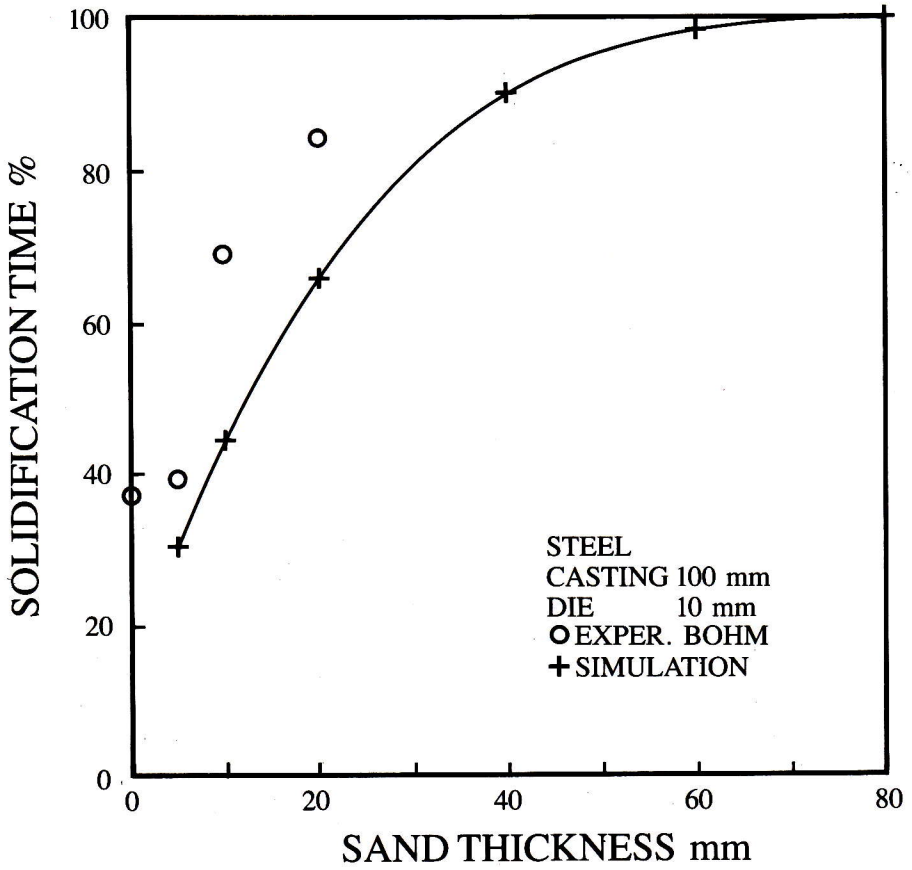
SOLIDIFICATION TIME %
100
80
60
40
20
0
0
20
40
60
80
SAND THICKNESS mm
STEEL
CASTING 100 mm
DIE 10 mm
O EXPER. BOHM
+ SIMULATION

Fig. 15

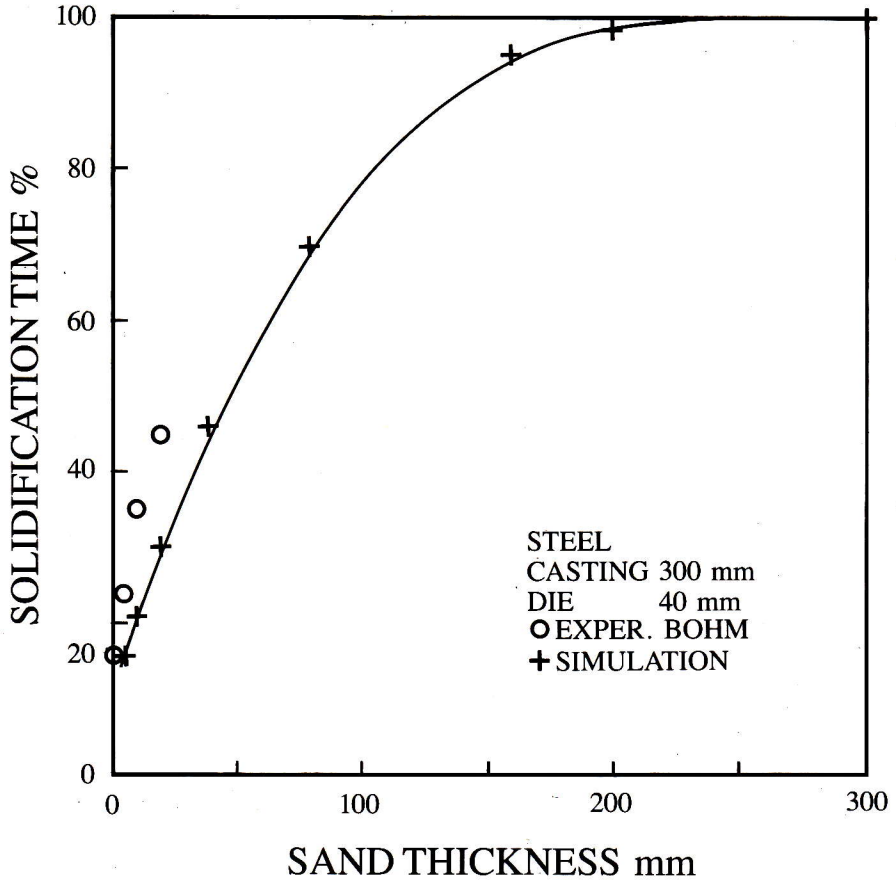
SOLIDIFICATION TIME %
100
80
60
40
20
0
0
100
200
300
SAND THICKNESS mm
STEEL
CASTING 300 mm
DIE 40 mm
O EXPER. BOHM
+ SIMULATION

Fig. 16

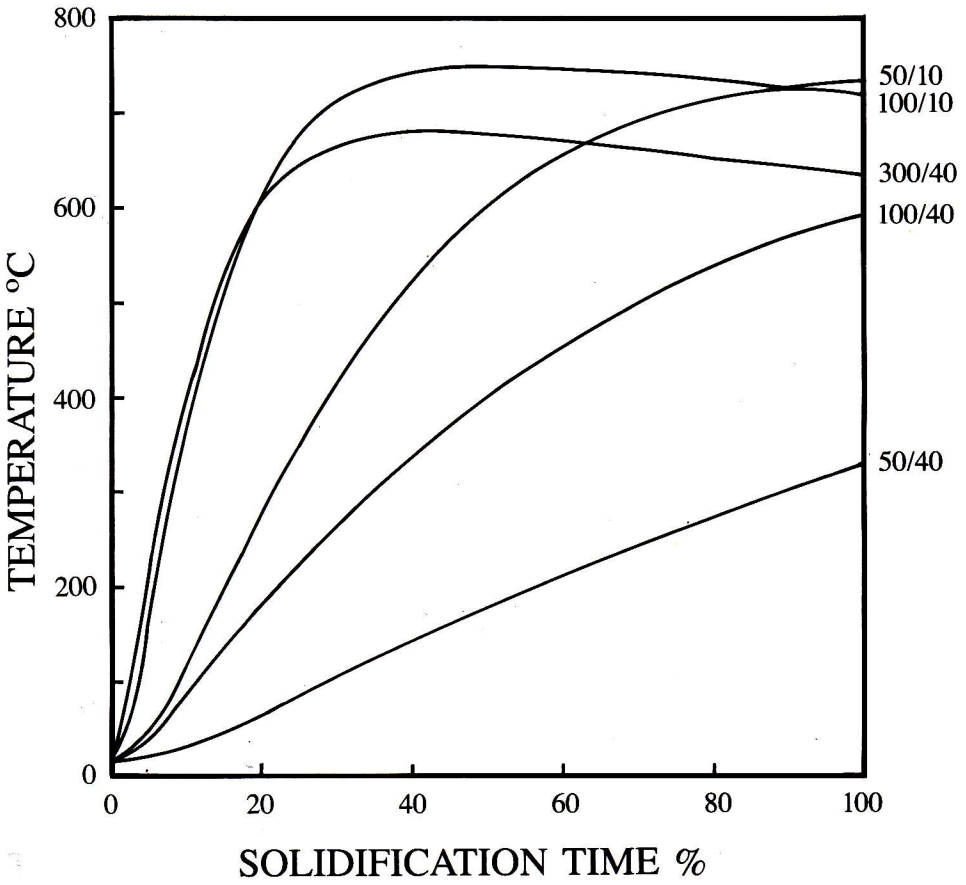
TEMPERATURE °C
800
600
400
200
0
0
20
40
60
80
100
SOLIDIFICATION TIME %
50/10
100/10
300/40
100/40
50/40

Fig. 17

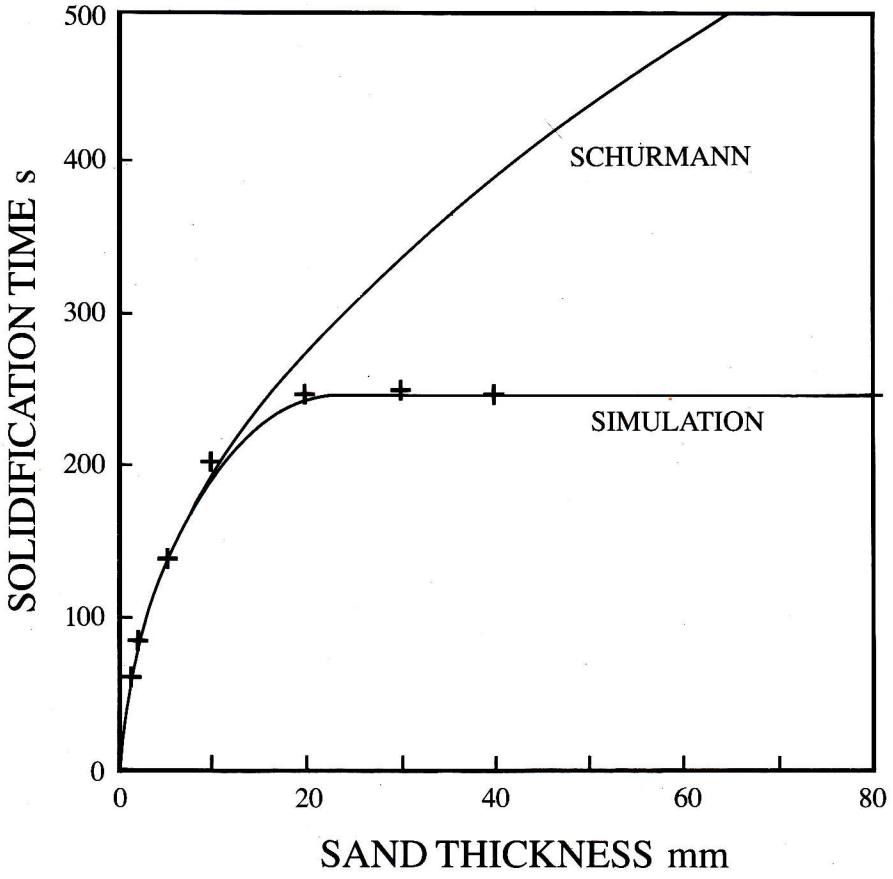
500
400
300
200
100
0
SOLIDIFICATION TIME s
SCHURMANN
SIMULATION
0
20
40
60
80
SAND THICKNESS mm

Fig. 18

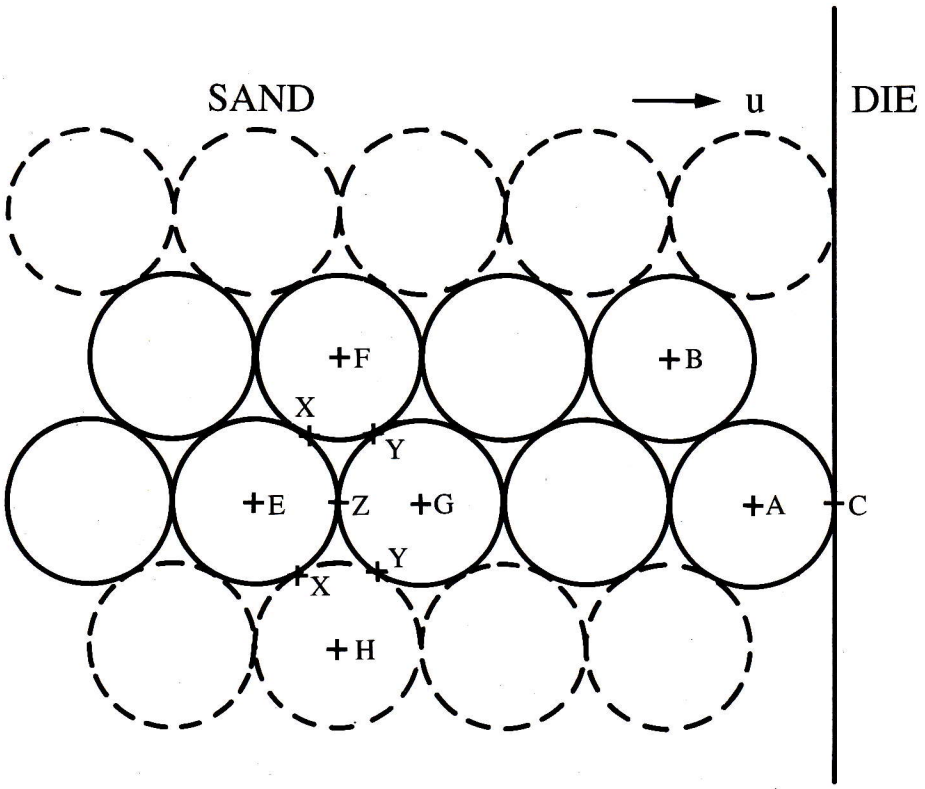
SAND
u
DIE
F
B
X
Y
E
Z
G
A
C
Y
X
H

Fig. 19

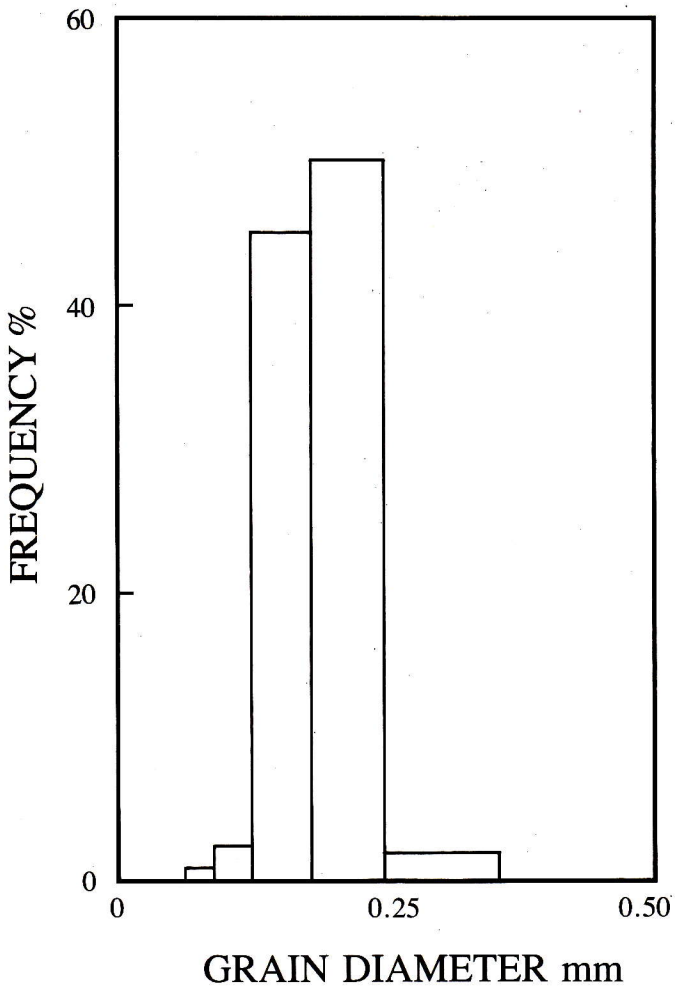
60
40
20
0
FREQUENCY %
0
0.25
0.50
GRAIN DIAMETER mm

Fig. 20

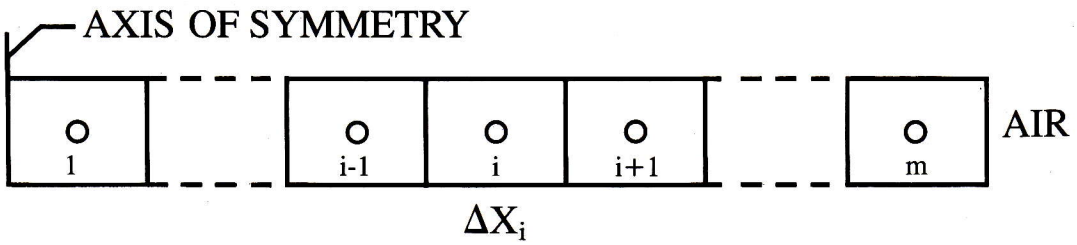
AXIS OF SYMMETRY
1
i-1
i
i+1
m
AIR
ΔX_i

Fig. 21